







## Pacific decadal variability over the last 2000 years and implications for climatic risk

Tessa R. Vance<sup>1</sup> <sup>✉</sup>, Anthony S. Kiem<sup>2</sup> , Lenneke M. Jong<sup>1,3</sup> , Jason L. Roberts<sup>1,3</sup> ,  
Christopher T. Plummer<sup>1</sup>, Andrew D. Moy<sup>1,3</sup> , Mark A. J. Curran<sup>1,3</sup> & Tas D. van Ommen<sup>1,3</sup> 

The Interdecadal Pacific Oscillation, an index which defines decadal climate variability throughout the Pacific, is generally assumed to have positive and negative phases that each last 20–30 years. Here we present a 2000-year reconstruction of the Interdecadal Pacific Oscillation, obtained using information preserved in Antarctic ice cores, that shows negative phases are short ( $7 \pm 5$  years) and infrequent (occurring 10% of the time) departures from a predominantly neutral-positive state that lasts decades ( $61 \pm 56$  years). These findings suggest that Pacific Basin climate risk is poorly characterised due to over-representation of negative phases in post-1900 observations. We demonstrate the implications of this for eastern Australia, where drought risk is elevated during neutral-positive phases, and highlight the need for a re-evaluation of climate risk for all locations affected by the Interdecadal Pacific Oscillation. The initiation and future frequency of negative phases should also be a research priority given their prevalence in more recent centuries.

<sup>1</sup> Australian Antarctic Program Partnership, Institute for Marine & Antarctic Studies, University of Tasmania, Hobart, TAS 7004, Australia. <sup>2</sup> Centre for Water, Climate & Land, University of Newcastle, Callaghan, NSW 2308, Australia. <sup>3</sup> Australian Antarctic Division, Kingston, TAS 7050, Australia.  
✉email: [tessa.vance@utas.edu.au](mailto:tessa.vance@utas.edu.au)

The relationship between Pacific decadal variability (PDV) and climate impacts such as Pacific Basin drought, flood, wildfire and tropical cyclone risk and global temperature has been extensively studied<sup>1–11</sup>. More recently, PDV has been implicated in pronounced changes in high latitude Southern Hemisphere and Antarctic climate, including abrupt declines in annual sea ice extent<sup>12</sup> and regional Antarctic surface air temperature warming<sup>13</sup> and cooling<sup>14</sup>, which has implications for global climate and ice mass balance projections. These studies are based on short (primarily satellite era) high latitude observations, which risk poorly characterising long-term variability<sup>15</sup>. It is therefore crucial to understand the behaviour of PDV both for regional climate outcomes that affect nations across the Pacific Basin, as well as the emerging evidence of abrupt and extreme changes affecting the Antarctic ice sheet and sea-ice.

The relative roles of internally generated versus atmospheric, radiative, volcanic and anthropogenic forcing in generating decadal variability, including modes such as the Interdecadal Pacific Oscillation (IPO) and Atlantic Multi-decadal Oscillation (AMO), has been argued for some time<sup>1,9,16–21</sup>. Regardless of the underlying cause, it is often assumed for both observed and palaeoclimate data that basin-wide PDV (as represented by the IPO) manifests as positive and negative phases of similar length, around 20–30 years<sup>1–4,22–24</sup>. An underlying, internally generated process causing decadal-scale oscillations such as the IPO in palaeoclimate studies has not been definitively identified. Recently, Mann et al.<sup>20,21</sup> identified volcanic forcing with multi-decadal pacing as the most likely trigger for the AMO using long observations and Last Millennium Ensemble climate simulations with and without forcing. These studies were built on previous model analyses suggesting that there may be competing natural and anthropogenic elements such as aerosol forcing of negative phases to multi-decadal modes<sup>18</sup> and their climate impacts such as shifts in precipitation<sup>25</sup>. While this raises questions about the role of internal mechanisms initiating decadal-scale modes such as the IPO and AMO, further studies including palaeoclimate reconstructions are needed to test the hypotheses that major volcanic eruptions and/or aerosol forcing generate quasi-periodic PDV.

Observational indices of the IPO used to quantify PDV span too few phase changes to definitively determine whether internal (deep ocean) modulation, stochastic (atmospheric) forcing of the surface ocean or some other mechanism drives the IPO<sup>8,9,19,26</sup>. Determining the frequency and distribution of IPO phases is crucial to understanding when and for how long the Pacific transitions to a different state, the underlying climate risk from these transitions and to reconcile climate projections with natural variability<sup>20,27,28</sup>. Multi-centennial, annually resolved reconstructions of PDV are needed to do this<sup>26,29</sup>.

A recent meta-analysis of existing reconstructions<sup>26</sup> determined that observation era IPO phase lengths are largely similar to those calculated from reconstructions that span recent centuries. However, the authors concluded that phase lengths/prevalence may have been different prior to the past 400–500 years, but the rarity of reconstructions longer than a few centuries precluded analysis of any multi-centennial change. Disagreement between reconstructions spanning recent centuries is also common, further hampering understanding of past PDV<sup>26,30,31</sup>.

Since this meta-analysis, we have analysed new ice core material, allowing the improvement and extension of our previous IPO reconstruction<sup>32</sup> derived from multiple records from deep ice core drilling at the summit of Law Dome, an extensively studied ice core site in East Antarctica. To develop this new reconstruction, we have refined annual dating and doubled reconstruction length by extending the Law Dome ice core records a further 1000 years in the past and further into the

observational era to span the Common Era (CE –10 to 2016) at annual resolution. We employed the same reconstruction methods developed in our previous work (Fig. 1a and ‘Methods’), which demonstrated highly skillful reconstructions to observational data (root mean square error = 0.408, see Vance et al.<sup>32</sup> for additional skill metrics) when the Law Dome ice core snowfall accumulation and seasonal sea salt aerosol records were used as input timeseries. The long reconstruction developed here exhibits a small, statistically significant trend of  $-0.0002$ ; however, the input ice core timeseries used in the reconstruction do not contain trends. In addition, we have reduced the risk of inhomogeneity due to decreasing sample resolution with time by maintaining sample resolution throughout the reconstruction and using a reconstruction method that is robust to missing or differently sampled data (see Methods). As a result, we do not recommend detrending the reconstruction developed here, as we consider the trend to be the result of more frequent and/or longer negative phases occurring in the last 500 years compared to the last 2000 years<sup>26</sup>. Nonetheless, we provide a statistical treatment of the detrended IPO reconstruction (see Supplementary Fig. 1) equivalent to Table 1. This demonstrates that the results we identify in this study are robust (see Supplementary Table 1).

The preservation of an IPO signal at Law Dome relies on decadal changes in mid-latitude wind speed and direction across the southern Indian Ocean leading to ENSO and IPO-specific signals in sea salt aerosols preserved in East Antarctic coastal snowfall (due to

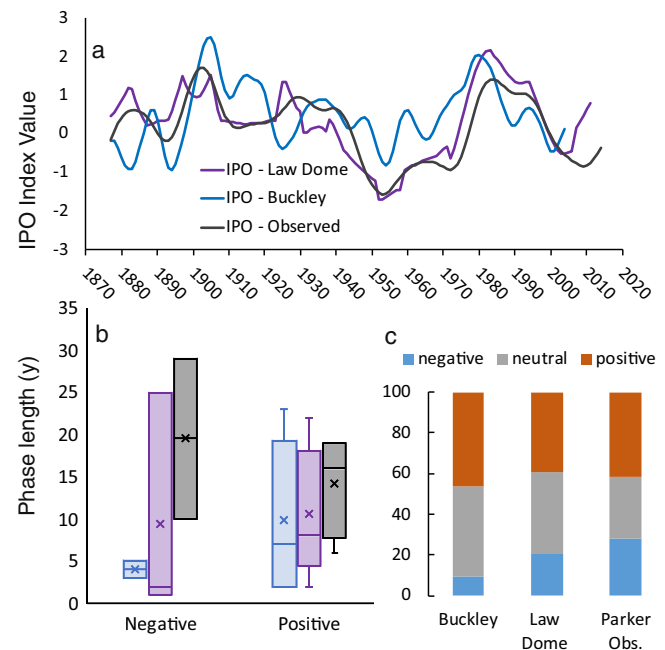


**Fig. 1** IPO Index and reconstruction characteristics over the observational period 1877–2014. **a** Comparison of observed Parker et al. IPO index (1877–2014, black), Buckley et al. IPO reconstruction (1877–2004, blue) and Law Dome IPO reconstruction (1877–2011, purple). **b** Box plots of positive and negative phase lengths (same colour scheme) for each timeseries over the same time period, with the caveat that only complete phases for any given series were included in the phase length analysis. Boxplot elements shown are the mean (X), median (midline), interquartile range (IQR—box boundaries) and data points outside the IQR but within 1.5× quartile range (whiskers). Numbers of phases were 6, 5 and 4 positive and 3, 2 and 2 negative for the Buckley et al., Law Dome and Observed series, respectively. **c** Percent time in each phase and neutral over the observed period (positive >0.5, neutral  $-0.5$  to  $0.5$  and negative  $<-0.5$ ). See Table 1 for more detail.

**Table 1** Phase length and frequency statistics for IPO observations and reconstructions over the stated periods.

Interval	Mean, standard deviation (years) Median, interquartile range (years) Percent time and (number of phases) over the specified interval		
	Positive (Index > 0.5)	Negative (Index < -0.5)	Neutral-positive (Index > -0.5)
Observed IPO (Parker et al. <sup>6</sup> ) 1877–2014	14.3, (6,13,19,19) 16 (7.8–19) 41.3% (4)	19.5 (29,10) <sup>a</sup> As above <sup>a</sup> 28.3% (2)	49 (70,28) <sup>a</sup> As above <sup>a</sup> 71.7% (2)
Buckley et al. <sup>29</sup> 1351–2004	10.2, 7.3 8, 4.5–14.5 51.2% (33)	5.2, 2.4 5, 3–7 11.9% (15)	36, 23.4 43.5, 12–50.5 88.1% (16)
Law Dome 1351–2004	7.4, 6.8 5.5, 3–8.5 29.0% (26)	7, 6.7 6, 1.5–10 13.8% (13)	40.7, 40.7 32.5, 6.8–69.3 86.2% (14)
Law Dome CE 1–2011	8.8, 7.7 6, 3–10 36.9% (84)	6.7, 5.2 6, 3–8.5 9.7% (29)	60.5, 56.2 48.5, 13.8–84 90.3% (30)

Note that the Parker et al. Index spans 1871–2020, but we calculate length and frequency statistics after excluding six years at either end to remove end effects in the 13 y Gaussian smoothed data we examine here (i.e. 1877–2014).  
<sup>a</sup>Only two negative and two neutral-positive phases or periods occur in observations, thus we present the mean and individual phase lengths instead of standard deviation for the observational data. Refer to Fig. 3 for distributions.

wind-initiated aerosolization across the ocean surface) and in the annual amount of precipitation (snowfall accumulation rate)<sup>32–38</sup>. Recently, a 654-y IPO reconstruction derived from pan-Pacific tree archives has been developed<sup>29</sup>. Despite their geographically distinct source regions and archives, the two reconstructions (Law Dome and Buckley et al.) visually show periods of reasonable agreement over their 654 y common period (CE 1351–2004)—for example, between 1350 and 1550 (Fig. 2a). However, they are not significantly correlated as the effective degrees of freedom is greatly reduced due to lag 1 autocorrelation in both reconstructions ( $r = 0.18$ ,  $N_{\text{eff}} = 30$ ) and coherence analysis identified little coherence between the two reconstructions at the 95% significance level (see methods for code/references). Disagreement between PDV reconstructions is common<sup>9,26,31</sup> and in this study primarily manifests as phase disagreement (one reconstruction is neutral where the other is positive/negative) or positive/negative phase swapping (reconstructions display opposite phases) with the latter occurring around 10% of the time (69/654 y, longest period 13 y). Importantly, however, both reconstructions appear predominantly positive–neutral and exhibit muted/insignificant spectral features at decadal to multi-decadal scales, suggesting neither reconstruction exhibits quasi- or true periodic variability. This constitutes the basis of our analysis: regardless of which reconstruction is ‘better’, we interrogate both reconstructions for what they can reveal about phase prevalence over the last two millennia given their apparent lack of periodic variability. Given their independence of origin they likely represent the best long, independent Common Era reconstructions of PDV to date, thus an examination of phase length, behaviour and implications therein is now possible. This work follows Mann et al.<sup>20</sup> and evaluates PDV phase length and prevalence over the Common Era using these PDV reconstructions. A case study of the implications for hydroclimatic variability in the SW Pacific (Australia) is developed and demonstrates that analysis of observations alone misrepresents PDV and its associated hydroclimatic risks.

**Results and discussion**

**Features of PDV in observations compared to the Common Era.** IPO positive or negative phases occur when the Parker et al. IPO index is above 0.5 or below -0.5 respectively, a threshold found to be robust in practice for climate outcomes such as rainfall and

streamflow variability and drought, flood, wildfire, tropical cyclone and storm surge risk<sup>1,3–5,39–43</sup>. The literature has commonly assumed phases last around 20–30 years<sup>1,3,4,9</sup>. The 13 y (half power) Gaussian smoothed Parker et al. Index spanning 1877–2014, with four positive (mean 14.3 y) and two negative (mean 19.5 y) phases nominally supports this (Table 1), albeit with little statistical confidence given the shortness of the observation period (Fig. 1b, c). The assumption of roughly equal periods in positive or negative phases fails when the reconstructions are examined in comparison to observations (Table 1 and Figs. 2c and 3). Regardless of time period or reconstruction, negative phases of the IPO occur far less frequently than positive phases (10–14% compared to 29–51%) and are shorter than observations would suggest (5–7 years compared to 19.5 years, Fig. 3a). In addition, the prevalence of negative phases as a percentage of time is higher in the last 661 years than in the prior 1350 years (Table 1 and Supplementary Table 1). As previously noted, spectral analyses of both reconstructions revealed no strong spectral features at inter- or multi-decadal bands. The two reconstructions demonstrate that the IPO exhibits a predominantly neutral-positive state (Table 1). Short, generally sub-decadal departures to negative occur with <10 to >150 years between negative phases, meaning the observational record misrepresents Common Era PDV. Our analysis suggests the IPO should be redefined to present PDV as a neutral-positive state of the Pacific Ocean with occasional departures to a negative state. We therefore introduce a new threshold to define PDV, ‘neutral-positive’ (Table 1), as it is pertinent to assessments of climatic risk such as the case study developed here. On balance, we suggest impacts particular to neutral-positive PDV should be of most concern to scientists and practitioners in the climatic risk communities as this better reflects the climate norm over the Common Era. However, the initiation of negative phases—whether internally generated, externally forced and/or anthropogenic—should receive attention from the climate and modelling communities to understand what initiates the Pacific to enter a negative state. Furthermore, any recent or future anthropogenic climate change effects on the occurrence or persistence of negative PDV phases requires investigation.

**Hydroclimatic risk case study: Eastern Australia.** Eastern Australia (Fig. 4) encompasses Australia’s three most populous cities,

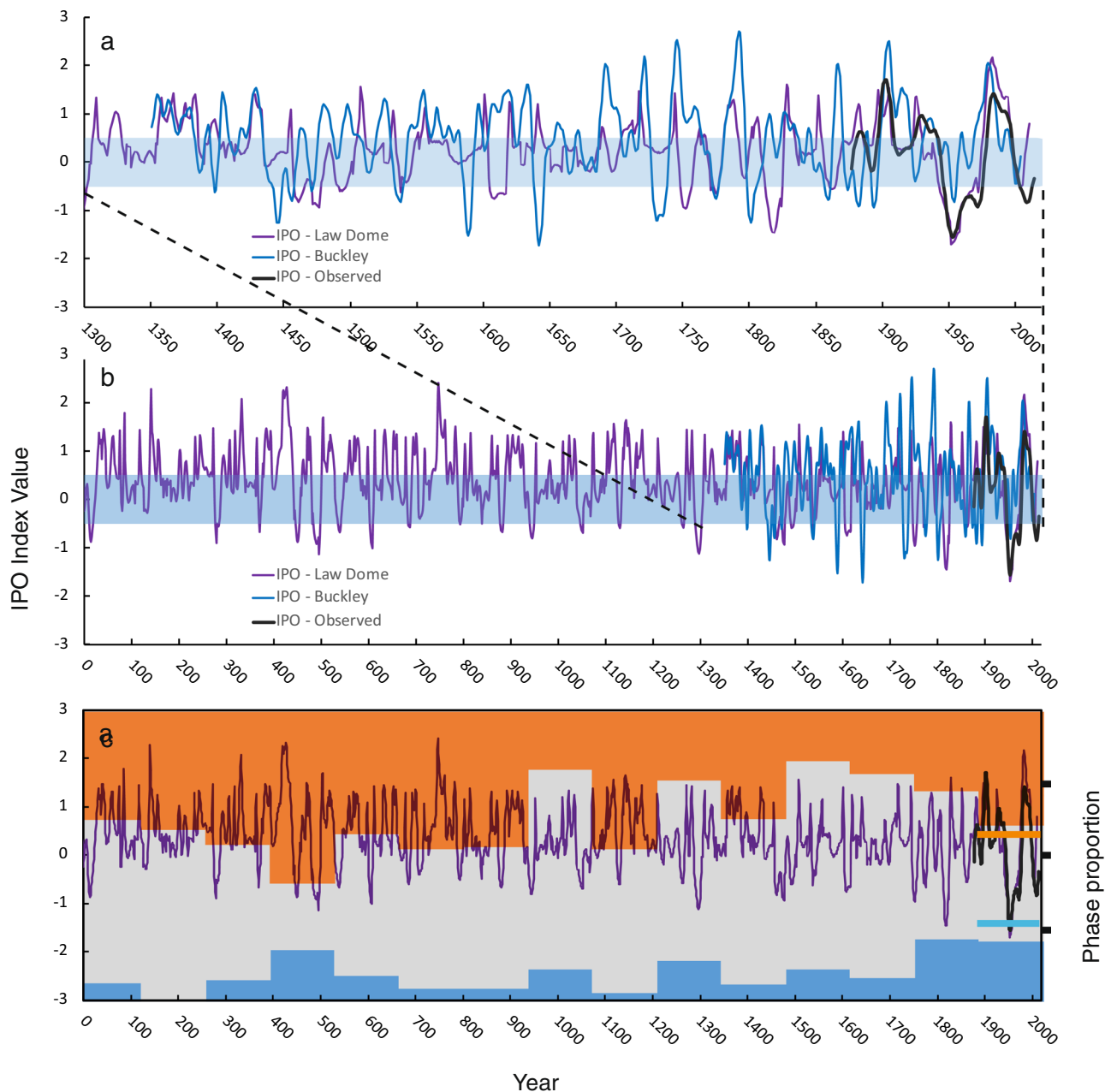


**Fig. 2 Comparison between the two IPO reconstructions and observational record.** The Buckley et al. reconstruction (1351–2004, blue) and the extended Law Dome reconstruction developed here (CE 1–2011, purple) are shown over their common period (**a**) and over the Common Era (**b**), with blue banding representing neutral IPO (0.5 to  $-0.5$ ). The lower panel of **c** shows the Law Dome reconstruction (purple) and instrumental record (black) over the Common Era with partitioning into phase proportions (positive, negative and neutral) in bands of 135 years (i.e. equivalent to the length of observations: 1877–2014, 1742–1876, 1607–1741, etc.). The phase proportion partitioning illustrates the time spent in each phase for equivalent observations length epochs. Note the earliest partition spans 127 years (CE 1–127). Blue indicates the proportion of time in the negative phase, grey is neutral and orange is positive. Blue and orange lines in the instrumental era represent phase proportions according to the observed IPO (1877–2014, negative 28.3%, neutral 30.4% and positive 41.3%). Black tick marks to the right identify quartiles. For reference, the Buckley et al. reconstruction spans the five recent 135 y bands and exhibits negative proportions of 10–14% and positive proportions of 47–58%.

largest and most important catchment and irrigated arable region (the Murray-Darling River Basin) and is home to 81% of Australia's population. This large and climatically diverse region, comprising around one-third the continental mass of Australia and spanning 34 degrees of latitude, demands the bulk of Australian water resources for irrigated farming, horticulture and urban needs as well as coal and other mining.

The hydroclimate of eastern Australia exhibits high inter-annual variability driven primarily by the El Niño-Southern Oscillation (ENSO), with PDV modulating the frequency and magnitude of ENSO events and their impact<sup>1,3,4</sup>. During negative IPO phases, La Niñas are more frequent and are typically associated with significantly higher rainfall which terminates droughts and recharges catchment moisture, groundwater and

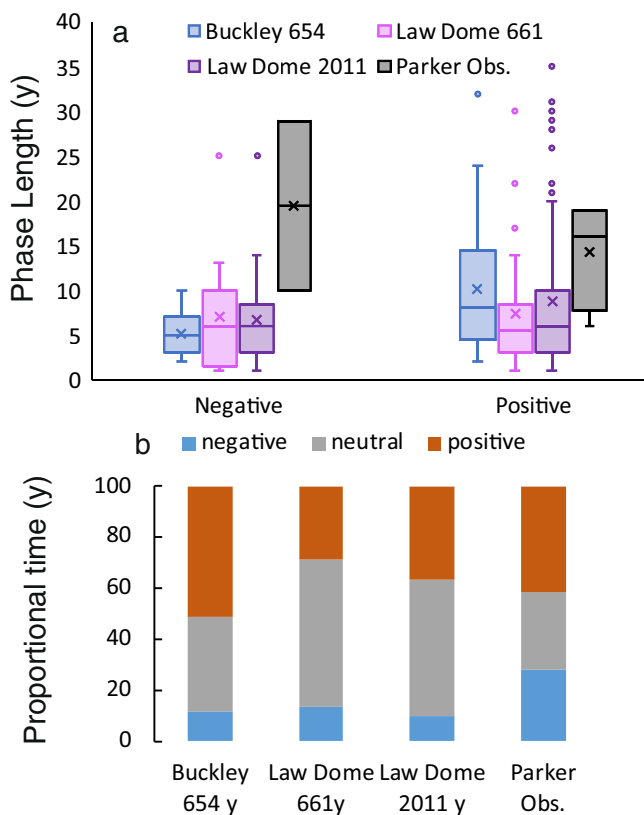


**Fig. 3** Phase lengths and proportional time. **a** Phase lengths in years for the observed IPO compared to the two reconstructions (with the Law Dome reconstruction examined from CE 1351 and for the Common Era). Boxplot elements shown are the mean (X), median (midline), IQR (box upper and lower boundaries) and data points outside the IQR but within  $1.5 \times$  quartile range (whiskers). Outliers ( $>1.5 \times$  IQR) are shown individually. **b** Proportional time in each of the three phases (positive ( $>0.5$ ), negative ( $<-0.5$ ) and neutral). See Table 1 for more detail.

reservoirs<sup>3,44–46</sup>. However, catchment spilling (and subsequent loss to storage) and catastrophic flooding also predominantly occur during negative IPO phases<sup>41</sup>.

Previous work has shown that negative and positive IPO phases have significantly different rainfall, drought, flood and wildfire distributions in Eastern Australia. However, the literature has assumed that 20–30 year drier IPO positive phases will be essentially balanced by wetter negative phases of similar length<sup>1,3–5</sup>. As we have shown, long reconstructions demonstrate negative IPO phases are in fact short and infrequent, which is likely to have profound implications for assessments of water security. To determine this, we tested for differences between rainfall distributions in:

1. Positive and negative phases<sup>3–5</sup>
2. Positive and neutral, as well as neutral and negative phases (to determine whether these distributions should be separated or grouped together).

First, consistent with the previous literature<sup>3–5</sup>, eastern Australian rainfall is significantly lower during positive IPO years than during negative IPO years (Fig. 4). The statistical probability of this difference varies by region, with the states of New South Wales and Queensland having the lowest probability that the distributions are the same. Second, for all domains of eastern Australia we found no evidence of difference between positive and neutral phase rainfall, that is, the two distributions

are statistically likely to be drawn from the same population. Third, we found that there is a higher probability that rainfall totals during negative phase years are significantly higher than during neutral IPO years. The degree of significance of this association varied by region, but on balance we propose that it is reasonable and useful to redefine rainfall distributions across eastern Australia into negative and neutral-positive IPO years. Finally, rainfall totals during neutral-positive IPO years are significantly lower than during negative phase years across all domains of eastern Australia ( $p < 0.01$ – $0.08$ , Fig. 4).

**Implications of predominantly neutral-positive IPO for Eastern Australia.** Given the predominance of neutral-positive PDV over the last 2000 years, we explored the implications for water resources in Eastern Australia in terms of reductions in total rainfall. As expected, there is little difference in the percentage rainfall reductions observed between negative to positive IPO years (6–14%) compared to negative to neutral-positive IPO years (7–12%) (Table 2). The same finding is evident in the station data for five (long and complete record) stations from the Australian Bureau of Meteorology high-quality station network (13–15% compared to 10–14%) (Table 2).

The ramifications of this are twofold. First, negative phases happen far less frequently than previously assumed, meaning any given regions' expected rainfall total should reflect what occurs during the predominantly neutral-positive IPO state, not the mean across all years. Second, hydroclimatic risk in positive IPO phases—e.g. increased drought risk across Eastern Australia—is statistically indistinguishable from the entire neutral-positive IPO period. The hydroclimatic risk from extreme wet events during IPO negative phases may therefore be less in a temporal sense (due to less frequent and/or shorter negative phases), but conversely, this means catchment re-wetting and the potential for drought terminating rainfall is also less likely for any given event in any given year.

Assuming mean annual rainfall is 7–12% less than during negative IPO phases also has implications for planning. Reductions between current mean annual rainfall estimates for all years versus IPO neutral-positive years are 2–4% (Table 2). However, due to the non-linearity in the relationship between rainfall and runoff (quantified using statistics from the twentieth century), this 2–4% decrease in annual rainfall in Eastern Australia corresponds to a 3–4 times greater (i.e. 6–16%) decrease in annual runoff/reservoir inflows<sup>47–49</sup>. While it is acknowledged that uncertainty exists about future hydroclimatic conditions, if neutral-positive IPO conditions do continue to dominate as they have over the past 2000 years, a 6–16% decrease in annual runoff/reservoir inflows represents a major threat to water security in eastern Australia.

The extreme fluctuations in Australia's hydroclimate linked to PDV are well established<sup>1,3–5</sup>. This work shows: (i) negative IPO phases do not occur as often or for as long as observations suggest, (ii) the assumption that the durations of negative IPO and positive IPO phases is similar is incorrect, and (iii) the mid-20<sup>th</sup> century negative IPO phase was highly unusual in length. As a result, the observational period appears unusual and is not reflective of the predominantly neutral-positive state of PDV over the last two millennia.

Palaeoclimate studies have indicated that Eastern Australian droughts of much longer duration have occurred prior to the twentieth and twenty-first centuries<sup>28,32,50–52</sup> and we suggest this is related to wetter negative phases being shorter and less frequent prior to the observed period. Much of eastern Australia's existing water infrastructure was planned and built in the decades following World War II, coinciding with the mid-twentieth



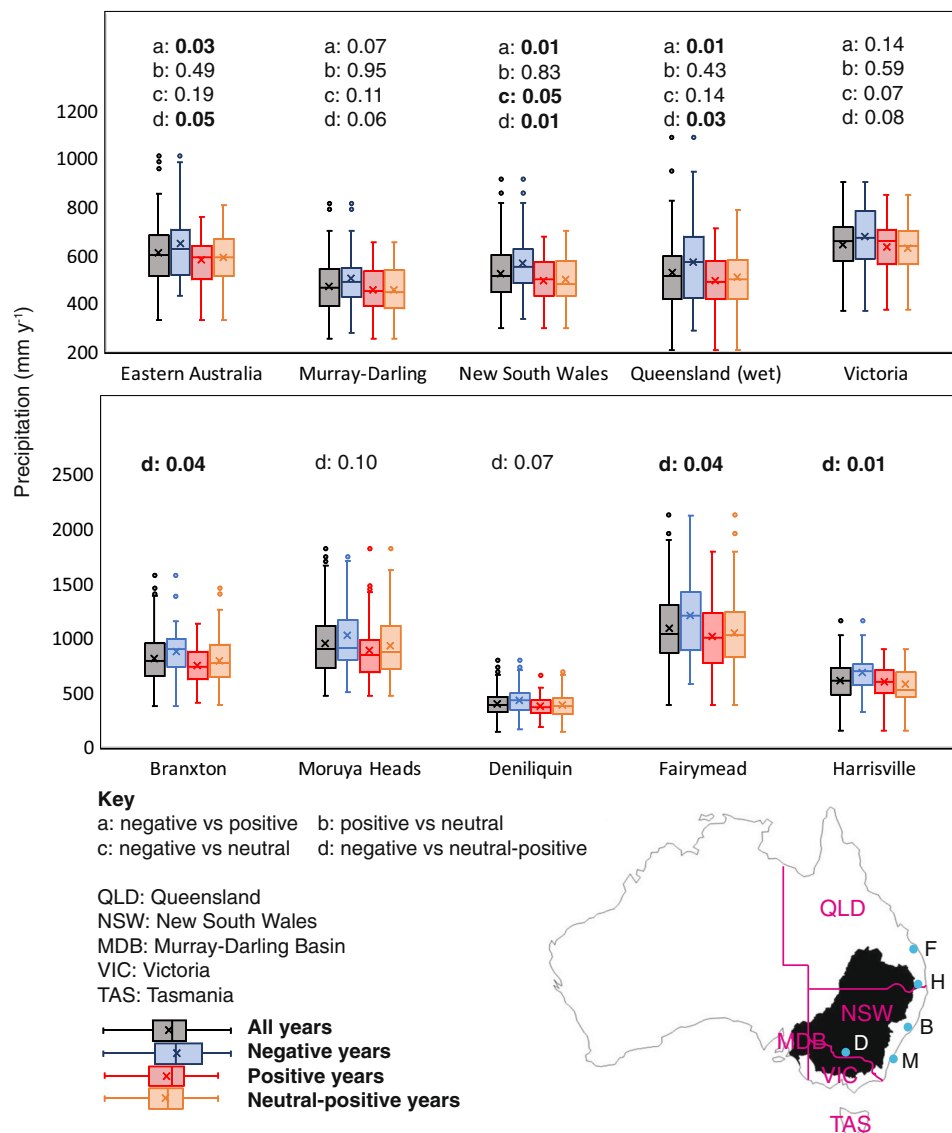


**Fig. 4 Rainfall distributions by IPO phase for Australian domains and long rainfall stations.** The rainfall distributions for each domain or station were calculated using annual (calendar year) total rainfall, which encompasses the water years for most regions except Queensland, which has a tropical (austral) summer wet season of October–April. Probabilities of no significant difference between rainfall distributions by IPO phase were tested using Welch’s *t* test, which is more robust to different sample sizes and variances than a standard Student’s *t* test. Note that there was little difference between the results for Welch’s versus Student’s *t* test. Probabilities for each domain are given above their respective boxplots ( $p < 0.05$  in bold), and the key identifies the distributions tested. Sample sizes for distributions over 1900–2014 are derived from the smoothed observed index (Fig. 1) and are negative: 39 y, positive: 47 y and neutral: 29 y. The key also indicates the domains tested, where Eastern Australia constitutes all the eastern states of Queensland, New South Wales (including the Australian Capital Territory), Victoria and the island of Tasmania. Annual total rainfall distributions in the catchment of Australia’s largest and most economically important river system, the Murray-Darling Basin (black) were also tested. Long rainfall stations are indicated with blue markers and station initial. Boxplot elements as per previous figures, with outliers ( $>1.5 \times \text{IQR}$ ) shown individually. See Table 2 for further statistics related to the distribution testing.

century negative IPO phase. This has profound implications for catchment statistics, which should be re-calculated to assume rainfall during neutral-positive IPO is the climatological norm.

## Conclusions

Mann et al.<sup>20</sup> built on a range of prior and contemporaneous work examining internal, natural/volcanic and anthropogenic aerosol forcing of decadal variability<sup>7–9,18,25</sup> and found that the past 150 years of observational data show little evidence of internal multi-decadal-scale modes of variability such as the AMO and by extension the IPO. In addition, further modelling

studies using Last Millennium Simulations required volcanic or anthropogenic forcing to produce decadal-scale variability<sup>21</sup>, work analogous to the identification of anthropogenic aerosol and volcanic forcing of PDV<sup>18</sup>. Nonetheless, the role that internal variability may play in IPO phase changes remains contentious<sup>9</sup>. Our study demonstrates that contrary to what has been assumed in the literature, Common Era PDV (as defined by reconstructions of the IPO) does not vary in a way that results in roughly equal periods of time in positive to negative phases. The implications of PDV exhibiting only infrequent departures to a negative state and the highly unusual nature of the mid-20<sup>th</sup> century

**Table 2 Annual (calendar year) or wet season mean rainfall differences between IPO phases for eastern Australian domains and stations.**

Domain or station	Period	Rainfall reductions (mm y <sup>-1</sup> )		Mean rainfall (mm y <sup>-1</sup> )		
		Negative-positive	Negative-neutral positive	All Years	Negative IPO	Neutral-positive IPO
Eastern Australia	1900–2014	65 (10%)	55 (9%)	609	647	592
Murray-Darling Basin	1900–2014	47 (9%)	47 (9%)	472	503	456
New South Wales	1900–2014	69 (12%)	67 (12%)	522	566	499
Queensland (wet season)	1900–2014	80 (14%)	67 (12%)	529	576	509
Victoria	1900–2014	40 (6%)	45 (7%)	645	674	629
Branxton Vineyard	1877–2014	131 (15%)	92 (10%)	812	882	790
Moruya Heads PS	1877–2014	142 (14%)	106 (10%)	955	1033	927
Deniliquin PO	1877–2014	55 (13%)	50 (12%)	399	433	383
Fairymead	1881–2014	175 (15%)	142 (12%)	1093	1192	1050
Harrisville PO	1897–2014	68 (10%)	92 (14%)	613	673	581

Eastern Australia is defined as the states of Queensland, New South Wales (incl. the Australian Capital Territory), Victoria, the island of Tasmania and most of the Murray-Darling Basin catchment (see Fig. 4). All rainfall data has been sourced from the Bureau of Meteorology High Quality Station network and regional/state totals (see 'Methods'). Rainfall mean differences are defined in mm y<sup>-1</sup> and percentage of total annual or seasonal rainfall and are without exception reductions in rainfall from negative to positive phases, or from negative to neutral-positive phases. We found no significant difference in eastern Australian rainfall distributions between the two observed negative IPO phases.

negative IPO phase have quantifiable implications, as phase changes and phase frequency have profound effects on climate risk and the management of the climate outcomes that occur across and beyond the Pacific Basin<sup>3,4,12–14,25</sup>.

We recommend the climate risks inherent to predominantly neutral-positive PDV should be the basis of overall risk assessment for climate risk scientists and practitioners investigating PDV-initiated climatic risk across the Pacific Basin. However, equally important is determining what initiates negative IPO phases in the climate system, the forcing required to maintain them, and any related anthropogenic aerosol and GHG effect. When considering decadal or longer projections of climate change, we suggest it is important to analyse the statistics of negative, positive and neutral-positive phases from long (> 500 years) palaeoclimate reconstructions of PDV, given the change in prevalence of negative phases in the last 661 years compared to the prior 1350 years.

Lastly, two possibilities for future PDV behaviour should be considered. One is that PDV will revert to its long-term predominantly neutral-positive state as represented by the Common Era reconstructions, meaning climate risk analyses using mid-20th century observations are questionable. Alternatively, the mid-20th century IPO negative phase anomaly (compared to the Common Era reconstruction) may actually represent a transition to a new normal, raising different but equivalent concerns about risk estimation in an era of more frequent and/or longer negative IPO phases.

Methods

**Ice core dating and data treatment.** Climate records from the Law Dome ice core have been intensively studied for more than three decades, and have proven pivotal to the current understanding of climate variability over the Common Era<sup>53</sup>. Law Dome is situated within the Wilkes Coast region of East Antarctica and is subject to intense synoptic weather systems generated in the Indo-Pacific sector of the Southern Ocean<sup>54</sup>. The Dome Summit South (DSS) Main ice core was drilled to bedrock (1200 m) near the summit of Law Dome (66.77° S, 112.81° E), between 1987 and 1994<sup>55</sup>. Subsequently, 10–30 m short ice cores have been drilled to overlap with the DSS Main core and the satellite era. The DSS composite record now reaches 2017, and is comprised of four overlapping individual records: DSS1617 (1990–2016), DSS97 (1888–1989), DSS99 1841–1887) and DSS Main which reaches 1841 and spans the Holocene, last glacial maximum and at its furthest, extends ~90,000 years. The annual layer-counted trace chemistry record of the DSS core spans the upper 852 m (currently 2332 years) after which layer thinning processes reduce seasonal sample resolution and annual layers are difficult to discern<sup>56</sup>. This study extends the seasonally resolved record to span CE –10 to

CE 2017 by layer counting seasonally resolved trace chemistry and isotopes between CE –10 to CE 2017.

Discrete ice core samples for trace chemistry and isotopic analysis were prepared under trace clean conditions in freezer laboratories<sup>56,57</sup>. Sea salts (Na<sup>+</sup> and Cl<sup>-</sup> ions) were analysed as part of a suite of trace ion species by ion chromatograph<sup>56,58</sup>. Warm season (austral summer) peaking water stable isotopes δ<sup>18</sup>oxygen and δDeuterium (δ<sup>18</sup>O, δD) for DSS97, DSS99 and DSS main were measured by isotope ratio mass spectrometry<sup>55</sup> or via Picarro L2130-i isotopic water analyser. Hydrogen peroxide (H<sub>2</sub>O<sub>2</sub>) was measured via fluorimetry<sup>59</sup>.

Dating of the 2026 year layer counted record was performed as follows. Briefly, independent layer counting used a multi-analyte approach of examining the high-resolution seasonally-varying species on a depth scale and assigning year boundaries for each year discerned. δ<sup>18</sup>O and δD exhibit mean maxima at DSS on 8 January ± 14 days. H<sub>2</sub>O<sub>2</sub> exhibits mean maxima on 21 December<sup>59,60</sup>. We also employed the winter maxima in trace sea salts: Cl<sup>-</sup>, Na<sup>+</sup>, Mg<sup>2+</sup>, and the summer maxima in non-sea-salt SO<sub>4</sub><sup>2-</sup> as well as the ratio of SO<sub>4</sub><sup>2-</sup>/Cl<sup>-</sup> for confirmatory dating<sup>56,60</sup>. The DSS layer counted timescale was derived independently without reference to volcanic eruptions. Reference horizons of known eruptions are however used to illustrate the counting error in the record; Mt Pinatubo (1992), Agung (1963), Tambora (1815), Samalas (1257), Unknown (422). The within-horizon dating errors of the DSS record derived from independent annual layer-counting are: Pinatubo–2016, 0 years, Agung–Pinatubo, 0 years, Tambora–Agung, 0 years, Samalas–Tambora, +1 year, Unknown 422–Simalas, +6/–11 years, 7 BCE–Unknown 422 CE, +7/–20 years. The uncertainty in the record increases with depth but is almost certainly less than indicated, that is, undercounting by 20 years would represent an extreme scenario dating error. To combat the reduction in sample resolution with depth due to thinning of annual layers, the annual chemistry sample resolution increased (by decreasing sample length) from 5 cm samples between 1300 and 2016 CE, to 3 cm samples from 980 to 1300 CE, and 2.5 cm between 10 BCE and 980. The mean sample resolution is highest near the surface (21 samples y<sup>-1</sup> for the period 1950–2016). The mean sample resolution from 1950–1600 is 12 samples y<sup>-1</sup>, decreasing to 11 y<sup>-1</sup> from 1600 to 1000 CE. By 7 BCE the mean resolution is 8 samples y<sup>-1</sup> for trace chemistry including sea salts. There is a 43 year period from 1568–1611 where the chemistry resolution decreases to 5 samples y<sup>-1</sup> due to a sampling error where 10 cm samples were produced instead of 5 cm samples. This does not impact dating as both δ<sup>18</sup>O and H<sub>2</sub>O<sub>2</sub> data were not affected by this and are available in higher resolution. Samples for δ<sup>18</sup>O record were at 5 cm resolution near the surface, decreasing to 1 cm at depth to preserve resolution. This enables the isotope record to maintain an average resolution of 15 samples y<sup>-1</sup>.

**Observational data treatment—IPO and rainfall.** We sourced an updated version of the IPO index at monthly resolution directly from Professor Chris Folland (email, 27 Jul 2007, personal communication) and Mr Andrew Colman<sup>6</sup>. The index provided spanned 1870 to July 2020, extending the reconstruction training period to include the recent negative IPO phase ending in 2014 (Fig. 1). More recently, the Tripole index (TPI), a measure of SST anomalies across three regions of the Pacific was developed to describe PDV<sup>24</sup>. Buckley et al.<sup>29</sup> found their reconstruction bore less resemblance to the TPI than to the Parker et al. index; equally, we wish to retain comparability with our previous work and that of Buckley et al.<sup>29</sup> and have used the IPO as defined by the Parker index. We produced an annually averaged

record (July–June), with 13 year (half power) Gaussian-smoothing ( $\sigma = 3.9$ ) as our reconstruction target, as per our previous reconstruction<sup>32</sup>.

We sourced long, quality-controlled rainfall station data sets held by the Australian Bureau of Meteorology in their High Quality station network, as well as Eastern Australian interpolated averages for the domains examined (<http://www.bom.gov.au/climate/change>). Rainfall stations chosen were based on length and completeness of the record, except for Harrisville Post office, which we have included as it is an indicator station for a catchment we have previously analysed for climate risk using palaeoclimate data<sup>28,61</sup>.

**Reconstructing the IPO.** This reconstruction follows the approach of our previous work<sup>32</sup> using the same but updated input data streams and extending into the past to produce a continuous reconstruction spanning the Common Era (CE 1 to CE 2011).

The timeseries used as inputs for the reconstruction were the log-transformed warm and cool season average sea salt concentrations (December–May and June–November respectively), and the annual snowfall accumulation rate in metres ice equivalent (m.i.e.), corrected by depth for the ice characteristics and strain rate of the DSS site<sup>32,33</sup>. None of the input time series contained significant trends. The sea salt data were derived from the chloride ( $\text{Cl}^-$ ) record, as the Law Dome sodium ( $\text{Na}^+$ ) record has critical data gaps that are not present in the chloride series. Testing has shown the sea salt ions in the Law Dome record, being a coastal wet deposition site, are essentially equivalent (Curran and Palmer<sup>58</sup>). In instances where there are small  $\text{Cl}^-$  data gaps and  $\text{Na}^+$  data does exist, we use the seawater ratio to produce an equivalent  $\text{Cl}^-$  concentration. We did not use seasonal concentrations for any year where missing ice core material or analytical instrument error meant that data comprising more than two of the six months required to derive the seasonal average for that year is missing or compromised. The raw sea salt data were log-transformed prior to deriving seasonal averages, as the sea salt data is long-tailed due to occasional high concentration events<sup>32,35</sup>.

The reconstruction presented here pre-processes these data streams in the same manner as previously. The warm and cool sea salt concentrations are combined into one time series using a 13 y window sliding correlation, which was previously shown to improve the skill of the reconstruction compared to the individual data streams<sup>32</sup>. Testing for this study showed that this improved skill is still apparent using our extended observation and ice core data. A Gaussian low-pass filter with  $\sigma = 3.9$  y (the equivalent of a 13 y full width half maximum) is applied to both data streams.

We have used two different reconstruction methods in this study. The same piece-wise linear fit (PLF) method<sup>62</sup> was used for comparison with our previous 2015 study. The number of basis functions was determined by minimising the root mean square error and generalised cross-validation scores of the reconstruction on the calibration period, with 9 basis functions selected as the optimal input, which is reduced to 8 by the pruning pass as part of the PLF routine. For the data presented in this study, we used a recently developed Gaussian kernel correlation reconstruction method which is robust for missing and unevenly sampled data<sup>63</sup>. For this method, the input data sets are linearised (using code included with the reconstruction method code) prior to being used in the reconstruction. This newer method calculates an ensemble of 2000 possible reconstructions, which results in a mean, upper and lower quartile value for each year (included in the data sets). Both methods show excellent agreement on the timing of the large negative IPO events. Spectral and coherence analyses were undertaken with the MTM toolkit<sup>64</sup>.

## Data availability

The Law Dome ice core data sets used as input series to reconstruct the IPO in this study are publicly available from the Australian Antarctic Data Centre (<https://data.aad.gov.au>), <https://doi.org/10.26179/5zm0-v192>. These data sets are described in a data paper submitted to Earth Systems Science Data (Jong et al., submitted). The IPO reconstruction data series is available from the Australian Antarctic Data Centre, <https://doi.org/10.26179/vk1n-5t86>.

## Code availability

All codes used to produce the Law Dome IPO reconstruction are available at <https://doi.org/10.5281/zenodo.5728527>. Spectral and coherence analyses were undertaken with the MTM toolkit code available here: <https://doi.org/10.26208/s591-rk61>

Received: 13 May 2021; Accepted: 12 January 2022;

Published online: 17 February 2022

## References

- Power, S., Casey, T., Folland, C., Colman, A. & Mehta, V. Interdecadal modulation of the impact of ENSO on Australia. *Clim. Dyn.* **15**, 319–324 (1999).

- Mantua, N. & Hare, S. The Pacific decadal oscillation. *J. Oceanogr.* **58**, 35–44 (2002).
- Kiem, A. S., Franks, S. W. & Kuczera, G. Multi-decadal variability of flood risk. *Geophys. Res. Lett.* **30**, 1035 (2003).
- Kiem, A. S. & Franks, S. W. Multi-decadal variability of drought risk - Eastern Australia. *Hydrol. Process.* **18**, 2039–2050 (2004).
- Verdon, D. C., Kiem, A. S. & Franks, S. W. Multi-decadal variability of forest fire risk - Eastern Australia. *Int. J. Wildland Fire* **13**, 165–171 (2004).
- Parker, D. et al. Decadal to multidecadal variability and the climate change background. *J. Geophys. Res. Atmos.* <https://doi.org/10.1029/2007JD008411> (2007).
- England, M. H. et al. Recent intensification of wind-driven circulation in the Pacific and the ongoing warming hiatus. *Nat. Clim. Change* <https://doi.org/10.1038/NCLIMATE2106> (2014).
- Dai, A., Fyfe, J. C., Xie, S.-P. & Dai, X. Decadal modulation of global surface temperature by internal climate variability. *Nat. Clim. Change* **5**, 555–559 (2015).
- Henley, B. J. Pacific decadal variability: indices, patterns and tropical-extratropical interactions. *Glob. Planet. Change* **155**, 42–55 (2017).
- Magee, A. D. & Verdon-Kidd, D. C. Historical variability of Southwest Pacific tropical cyclone counts since 1855. *Geophys. Res. Lett.* <https://doi.org/10.1029/2019GL082900> (2019).
- Gray, J. L., Verdon-Kidd, D. C., Callaghan, J. & English, N. B. On the recent hiatus of tropical cyclones landfalling in NSW, Australia. *J. South. Hemisph. Earth Syst. Sci.* **70**, 180–192 (2020).
- Meehl, G., Arblaster, J., Bitz, C., Chung, C. & Teng, H. Antarctic sea-ice expansion between 2000 and 2014 driven by tropical Pacific decadal climate variability. *Nat. Geosci.* **9**, 590–595 (2016).
- Clem, K. R. et al. Record warming at the South Pole during the past three decades. *Nat. Clim. Change* <https://doi.org/10.1038/s41558-020-0815-z> (2020).
- Turner, J. et al. Absence of 21st century warming on Antarctic Peninsula consistent with natural variability. *Nature* **535**, 411–415 (2016).
- Jones, J. M. et al. Assessing recent trends in high-latitude Southern Hemisphere surface climate. *Nat. Clim. Change* **6**, 917–926 (2016).
- Newman, M., Compo, G. P. & Alexander, M. A. ENSO-forced variability of the Pacific Decadal Oscillation. *J. Clim.* **16**, 3853–3857 (2003).
- Liu, Z. Y. Dynamics of interdecadal climate variability: a historical perspective. *J. Clim.* **25**, 1963–1995 (2012).
- Smith, D. M. et al. Role of volcanic and anthropogenic aerosols in the recent global surface warming slowdown. *Nat. Clim. Change* **6**, 936–941 (2016).
- Lou, J., Holbrook, N. J. & O’Kane, T. J. South Pacific decadal climate variability and potential predictability. *J. Clim.* **32**, 6051–6069 (2019).
- Mann, M. E., Steinman, B. A. & Miller, S. K. Absence of internal multidecadal and interdecadal oscillations in climate model simulations. *Nat. Commun.* **11**, 49 (2020).
- Mann, M. E., Steinman, B. A., Brouillette, D. J. & Miller, S. K. Multidecadal climate oscillations during the past millennium driven by volcanic forcing. *Science* **371**, 1014–1019 (2021).
- Folland, C. K., Renwick, J. A., Salinger, M. J. & Mullen, A. B. Relative influences of the Interdecadal Pacific Oscillation and ENSO on the South Pacific Convergence Zone. *Geophys. Res. Lett.* **29**, 1643 (2002).
- D’Arrigo, R. & Wilson, R. On the Asian expression of the PDO. *Int. J. Climatol.* **26**, 1607–1617 (2006).
- Henley, B. et al. A tripole index for the Interdecadal Pacific Oscillation. *Clim. Dyn.* **45**, 3077–3090 (2015).
- Bonfils, C. J. W. et al. Human influence on joint changes in temperature, rainfall and continental aridity. *Nat. Clim. Change* **10**, 726–731 (2020).
- Zhang, L., Kuczera, G., Kiem, A. S. & Willgoose, G. R. Using paleoclimate reconstructions to analyse hydrological epochs associated with Pacific decadal variability. *Hydrol. Earth Syst. Sci.* **22**, 6399–6414 (2018).
- Collins, M. et al. in *Climate Change 2013: The Physical Science Basis* (eds Stocker, T. F. et al.) 1029–1136 (Cambridge University Press, 2013).
- Armstrong, M. S., Kiem, A. S. & Vance, T. R. Comparing instrumental, palaeoclimate and projected rainfall data: Implications for water resources management and hydrological modelling. *J. Hydrol.* **31**, 100728 (2020).
- Buckley, B. M. et al. Interdecadal Pacific Oscillation reconstructed from trans-Pacific tree rings: 1350–2004 CE. *Clim. Dyn.* **53**, 3181–3196 (2019).
- Verdon, D. C. & Franks, S. W. Long-term behaviour of ENSO: Interactions with the PDO over the past 400 years inferred from palaeoclimate records. *Geophys. Res. Lett.* <https://doi.org/10.1029/2005GL025052> (2006).
- Porter, S. E., Mosley-Thompson, E., Thompson, L. G. & Wilson, A. B. Reconstructing a Pacific Interdecadal Oscillation Index from a Pacific basin-wide collection of ice core records. *J. Clim.* **34**, 3839–3852 (2021).
- Vance, T. R., Roberts, J. L., Plummer, C. T., Kiem, A. S. & van Ommen, T. D. Interdecadal Pacific variability and eastern Australian megadroughts over the last millennium. *Geophys. Res. Lett.* **42**, 129–137 (2015).
- Roberts, J. et al. A 2000-year annual record of snow accumulation rates for Law Dome, East Antarctica. *Clim. Past* **11**, 697–707 (2015).



34. van Ommen, T. D. & Morgan, V. Snowfall increase in coastal East Antarctica linked with southwest Western Australian drought. *Nat. Geosci.* **3**, 267 (2010).
35. Vance, T. R., Ommen, T. D. V., Curran, M. A. J., Plummer, C. T. & Moy, A. D. A millennial proxy record of ENSO and Eastern Australian rainfall from the Law Dome Ice Core, East Antarctica. *J. Clim.* **26**, 710–725 (2013).
36. Vance, T. R. et al. Optimal site selection for a high-resolution ice core record in East Antarctica. *Clim. Past* **12**, 595–610 (2016).
37. Udy, D. G., Vance, T. R., Kiem, A. S., Holbrook, N. J. & Curran, M. A. J. Links between large-scale modes of climate variability and synoptic weather patterns in the southern Indian Ocean. *J. Clim.* **34**, 883–899 (2021).
38. Crockart, C. K. et al. El Niño–Southern Oscillation signal in a new East Antarctic ice core, Mount Brown South. *Clim. Past* **17**, 1795–1818 (2021).
39. Stevens, H. R. & Kiem, A. S. Developing hazard lines in response to coastal flooding and sea level change. *Urban Pol. Res.* **32**, 341–360 (2014).
40. Magee, A. D., Verdon-Kidd, D. C., Diamond, H. J. & Kiem, A. S. Influence of ENSO, ENSO Modoki, and the IPO on tropical cyclogenesis: a spatial analysis of the southwest Pacific region. *Int. J. Climatol.* **37**, 1118–1137 (2017).
41. McMahon, G. M. & Kiem, A. S. Large floods in South East Queensland, Australia: is it valid to assume they occur randomly? *Austral. J. Water Resour.* **22**, 4–14 (2018).
42. Deb, P. et al. Causes of the Widespread 2019–2020 Australian Bushfire Season. *Earth's Future* **8**, e2020EF001671 (2020).
43. Magee, A. D. & Kiem, A. S. Using indicators of ENSO, IOD, and SAM to improve lead time and accuracy of tropical cyclone outlooks for Australia. *J. Appl. Meteorol. Climatol.* <https://doi.org/10.1175/jamc-d-20-0131.1> (2020).
44. van Dijk, A. I. J. M. et al. The millennium drought in southeast Australia (2001–2009): natural and human causes and implications for water resources, ecosystems, economy and society. *Water Resour. Res.* **49**, 1–18 (2013).
45. Johnson, F. et al. Natural hazards in Australia: floods. *Clim. Change* **139**, 21–35 (2016).
46. Holgate, C. M., van Dijk, A. I. J. M., Evans, J. P. & Pitman, A. J. Local and remote drivers of southeast Australian drought. *Geophys. Res. Lett.* <https://doi.org/10.1029/2020GL090238> (2020).
47. Chiew, F. S. H. Estimation of rainfall elasticity of streamflow in Australia. *Hydrol. Sci. J.* **51**, 613–625 (2006).
48. Wooldridge, S. A., Franks, S. W. & Kalma, J. D. Hydrological implications of the Southern Oscillation: variability of the rainfall-runoff relationship. *Hydrol. Sci. J.* **46**, 73–88 (2001).
49. Kiem, A. S. & Verdon-Kidd, D. C. Climatic drivers of Victorian streamflow: is ENSO the dominant influence? *Austral. J. Water Resour.* **13**, 17–29 (2009).
50. Flack, A. L., Kiem, A. S., Vance, T. R., Tozer, C. R. & Roberts, J. L. Comparison of published palaeoclimate records suitable for reconstructing annual to sub-decadal hydroclimatic variability in eastern Australia: implications for water resource management and planning. *Hydrol. Earth Syst. Sci.* **24**, 5699–5712 (2020).
51. Barr, C. et al. Holocene El Niño–Southern Oscillation variability reflected in subtropical Australian precipitation. *Sci. Rep.* **9**, 1627 (2019).
52. Tozer, C. R. et al. Reconstructing pre-instrumental streamflow in Eastern Australia using a water balance approach. *J. Hydrol.* **558**, 632–646 (2018).
53. Etheridge, D. M., Steele, L. P., Lagenfelds, R. L. & Francey, R. J. Natural and anthropogenic changes in atmospheric CO<sub>2</sub> over the last 1000 years from air in Antarctic ice and firn. *J. Geophys. Res.* **101**, 4115–4128 (1996).
54. Massom, R. A. et al. Precipitation over the Interior East Antarctic Ice Sheet related to midlatitude blocking-high activity. *J. Clim.* **17**, 1914–1928 (2004).
55. Morgan, V. et al. Site information and initial results from deep ice drilling on Law Dome. *J. Glaciol.* **43**, 3–10 (1997).
56. Plummer, C. T. et al. An independently dated 200-yr volcanic record from Law Dome, East Antarctica, including a new perspective on the dating of the c. 1450s eruption of Kuwae, Vanuatu. *Clim. Past* **8**, 1929–1940 (2012).
57. Curran, M. A. J., van Ommen, T. D., Morgan, V. I., Phillips, K. L. & Palmer, A. S. Ice core evidence for Antarctic sea ice decline since the 1950s. *Science* **302**, 1203–1206 (2003).
58. Curran, M. A. J. & Palmer, A. S. Suppressed ion chromatography method for the routine determination of ultra low level anions and cations in ice cores. *J. Chromatogr. A* **919**, 107–113 (2001).
59. van Ommen, T. D. & Morgan, V. Peroxide concentrations in the Dome Summit South ice core, Law Dome, Antarctica. *J. Geophys. Res.* **101**, 15,147–15,152 (1996).
60. van Ommen, T. D. & Morgan, V. Calibrating the ice core paleothermometer using seasonality. *J. Geophys. Res.* **102**, 9351–9357 (1997).
61. Kiem, A. S. et al. Learning from the past – using palaeoclimate data to better understand and manage drought in South East Queensland (SEQ), Australia. *J. Hydrol. Reg. Stud.* <https://doi.org/10.1016/j.ejrh.2020.100686> (2020).
62. Friedman, J. H. Multivariate adaptive regression splines. *Ann. Stat.* **19**, 1–67 (1991).
63. Roberts, J. L. et al. Reconciling unevenly sampled palaeoclimate proxies: a Gaussian kernel correlation multiproxy reconstruction. *J. Environ. Inform.* <https://doi.org/10.3808/jei.201900420> (2019).
64. Mann, M. E. & Lees, J. Robust estimation of background noise and signal detection in climatic time series. *Clim. Change* **33**, 409–455 (1996).

## Acknowledgements

This work was funded by an Australian Research Council Discovery Project DP180102522, the Australian Research Council Special Research Initiative for Antarctic Gateway Partnership SR140300001 and past funding from the Antarctic Climate & Ecosystems Cooperative Research Centre (ACE CRC, 2010–2019). This work contributes to Australian Antarctic Science projects 4061, 4062, 4537 and 4414. We thank Brendan Buckley for pan-Pacific IPO reconstruction data and Chris Folland and Andrew Colman for IPO index data.

## Author contributions

T.R.V. designed the study and led the analysis, interpretation and writing. T.R.V. and A.S.K. designed the case study analysis and neutral-positive/negative IPO framework. L.M.J. and J.L.R. designed the reconstruction methods and developed the IPO reconstruction. C.T.P. led the dating of the Common Era ice core records with M.A.J.C., A.D.M. and T.D.v.O. All authors contributed to ice core data analyses and discussions during manuscript preparation.

## Competing interests

The authors declare no competing interests.

## Additional information

**Supplementary information** The online version contains supplementary material available at <https://doi.org/10.1038/s43247-022-00359-z>.

**Correspondence** and requests for materials should be addressed to Tessa R. Vance.

**Peer review information** *Communications Earth & Environment* thanks Chris Folland and the other anonymous reviewer(s) for their contribution to the peer review of this work. Primary handling editors: Joy Merwin Monteiro, Joe Aslin.

**Reprints and permission information** is available at <http://www.nature.com/reprints>

**Publisher's note** Springer Nature remains neutral with regard to jurisdictional claims in published maps and institutional affiliations.



**Open Access** This article is licensed under a Creative Commons Attribution 4.0 International License, which permits use, sharing, adaptation, distribution and reproduction in any medium or format, as long as you give appropriate credit to the original author(s) and the source, provide a link to the Creative Commons license, and indicate if changes were made. The images or other third party material in this article are included in the article's Creative Commons license, unless indicated otherwise in a credit line to the material. If material is not included in the article's Creative Commons license and your intended use is not permitted by statutory regulation or exceeds the permitted use, you will need to obtain permission directly from the copyright holder. To view a copy of this license, visit <http://creativecommons.org/licenses/by/4.0/>.

© The Author(s) 2022